Bulletin of the Seismological Society of America, Vol. 106, No. 6, pp. 2784–2795, December 2016, doi: 10.1785/0120160086

Possible Indicator of a Strong Isotropic Earthquake Component: Example of Two Shallow Earthquakes in Greece

by Dana Křížová, Jiří Zahradník, and Anastasia Kiratzi

Abstract For routine practice, we need simple tools to reliably identify earthquakes with large isotropic (ISO) components. This study aims to highlight a possible indicator. Non-double-couple (non-DC) components of moment tensors (MTs) play a key role in our understanding of faulting earthquake processes and/or in identifying explosions. As opposed to DC components of the calculated seismic source model, the non-DC components (compensated linear vector dipole and ISO) are more vulnerable to errors in location, inaccurate velocity modeling, and noise. Methods for analyzing resolvability of ISO are relatively complicated. We propose a simple procedure to identify an earthquake with a strong ISO component. Recent MT determinations include space and time grid search of the centroid position, mainly the depth and time. The centroid is identified with a trial source position that maximizes correlation between real and synthetic waveforms. In synthetic tests with varying ISO percentage, we compare the correlation-depth dependence for two types of MT inversion: full and deviatoric. We show that in the inversion of data with a significant ISO component under the deviatoric assumption (i.e., when ISO is neglected), we might obtain an inaccurate centroid depth. However, when we make the grid search twice, under the deviatoric-MT and full-MT assumptions, and compare the results, we can obtain an indication of the significant ISO and avoid depth bias. This straightforward method is applied to two shallow earthquakes in Greece (the 27 January 2012 M_w 5.3 Cretan Sea earthquake and the 26 June 2009 M_w 4.9 Santorini earthquake).

Introduction

Moment tensor (MT) calculations today belong to seismological routine. Few agencies (e.g., GeoForschungsZentrum [GFZ]) calculate the full MT, whereas most others (including Global Centroid Moment Tensor [CMT] and U.S. Geological Survey [USGS]) usually determine only the deviatoric MT, neglecting the isotropic (ISO) component. The double-couple (DC) part of MT is standard (useful and important) output from MT calculations. It is commonly parameterized by means of the strike, dip, and rake angles, expressing the so-called focal mechanism (or fault-plane solution). The focal mechanism is relatively stable with respect to inaccuracies of the routinely available velocity models and also with respect to possible errors in the assumed source positions. Nevertheless, to make the focal mechanism even more reliable, the source (centroid) position and time are sometimes jointly inverted with the mechanism. Contrary to the focal mechanism, the non-DC components of MT are difficult to determine because they are unstable. It means that they vary a lot with small changes of the velocity model, source–station configuration, and frequency range, among others.

Previous work has focused on research of non-DC components, their limited reliability, error assessment, and similar issues, starting in the 1990s (Vasco, 1990; Dufumier and Rivera, 1997; Julian *et al.*, 1998). Here, we focus on shallow earthquakes, but studies for deep earthquakes are available (Kawakatsu, 1996; Vavryčuk, 2004). Earthquake swarms often include non-DC events. For example, in West Bohemia (Czech Republic), the non-DC components could be caused by fluid injection (Horálek *et al.*, 2002), and a number of earthquakes in that region can be classified as tensile earthquakes (Vavryčuk, 2011). Earthquakes with noticeable compensated linear vector dipole (CLVD) or ISO components could be observed during borehole experiments. Vavryčuk *et al.* (2008) discovered two main types of these events. One type looked like a response to injection, while the other could be connected with anisotropy of rocks.

Full-MT calculation provides a pathway to understand the fracturing process (Song and Toksöz, 2011) and how to differentiate natural from induced seismicity (Ford *et al.*, 2009; Cesca *et al.*, 2013). The full-MT inversion is useful in the studies of nuclear explosions (Minson and Dreger, 2008). Non-DC components can be substantial during volcanic earthquakes, for example, Long Valley Caldera in California (Foulger *et al.*, 2004; Templeton and Dreger, 2006). Among several types of non-DC volcanic events, it is worth mentioning the case of vertical-CLVD earthquakes (Shuler *et al.*, 2013), or earthquakes with a large non-DC component but missing the ISO component (Tkalčić *et al.*, 2009). Recently, Mustać and Tkalčić (2016) used a nonlinear Bayesian inver-

sion in which noise represents a free parameter and is implemented via empirical covariance matrix.

Despite the efforts invested into non-DC components, in practice users are still confused regarding practical questions, as for example the following: is it better to always calculate full MT, while we know that only its strike/dip/rake (and moment) are reliable? Is it instead preferable to calculate the deviatoric MT? Is the percentage of the DC part (hereafter, DC%) well determined if derived from the deviatoric MT? More specifically, the objective of this article is to analyze how the deviatoric constraint affects the MT inversion results such as the DC%, the centroid depth, and the strike/dip/rake angles. The main innovative product is a simple indicator of events with strong ISO components, easily applicable to routine observatory practice.

This article is structured as follows: first, we briefly summarize methods that we use to invert waveforms into MT. Then, we introduce two real events that occurred in Greece: the 2012 Cretan Sea and the 2009 Santorini earthquakes. Next, we perform synthetic tests using the same source–station geometry as for the two real events. We vary the strength of the non-DC components and compare the full-MT and deviatoric-MT inversions. We arrive at a hypothesis that events with a significant ISO component can be detected by a simple comparison of the full-MT and deviatoric-MT inversions, and that the centroid depth determination of such events, under deviatoric constraint, may be highly inaccurate. Finally, we return to the two real events and show that the Santorini (volcanic) earthquake has a significant ISO component, whereas ISO of the Cretan Sea earthquake seems to be negligible (i.e., the latter appears to be a common tectonic earthquake).

Method

Basic Equations

Moment tensor $\mathbf{M}$ of an earthquake is expressed in the form of a linear combination of six elementary (dimensionless) moment tensors $\mathbf{M}^i$:

$$\mathbf{M}_{pq} = \sum_{i=1}^{6} a_i \mathbf{M}^i_{pq}. \tag{1}$$

We use the elementary tensors as in the discrete-wavenumber code AXITRA of Coutant (1989):

$$\mathbf{M}^1 = \begin{pmatrix} 0 & 1 & 0 \\ 1 & 0 & 0 \\ 0 & 0 & 0 \end{pmatrix} \quad \mathbf{M}^2 = \begin{pmatrix} 0 & 0 & 1 \\ 0 & 0 & 0 \\ 1 & 0 & 0 \end{pmatrix}$$
$$\mathbf{M}^3 = \begin{pmatrix} 0 & 0 & 0 \\ 0 & 0 & -1 \\ 0 & -1 & 0 \end{pmatrix} \quad \mathbf{M}^4 = \begin{pmatrix} -1 & 0 & 0 \\ 0 & 0 & 0 \\ 0 & 0 & 1 \end{pmatrix}$$
$$\mathbf{M}^5 = \begin{pmatrix} 0 & 0 & 0 \\ 0 & -1 & 0 \\ 0 & 0 & 1 \end{pmatrix} \quad \mathbf{M}^6 = \begin{pmatrix} 1 & 0 & 0 \\ 0 & 1 & 0 \\ 0 & 0 & 1 \end{pmatrix}. \tag{2}$$

The $\mathbf{M}^1$–$\mathbf{M}^5$ tensors represent five DC focal mechanisms, whereas $\mathbf{M}^6$ is a purely ISO source. The a-coefficients in equation (1), or simply a, are related to $\mathbf{M}$ as

$$\mathbf{M} = \begin{pmatrix} -a_4 + a_6 & a_1 & a_2 \\ a_1 & -a_5 + a_6 & -a_3 \\ a_2 & -a_3 & a_4 + a_5 + a_6 \end{pmatrix}. \tag{3}$$

The moment trace is related with just a single a-coefficient, $a_6 = \mathrm{tr}(\mathbf{M})/3$. The scalar seismic moment is defined by Silver and Jordan (1982) as

$$\mathbf{M}_0 = \sqrt{\frac{\sum_{p=1}^{3}\sum_{q=1}^{3}(\mathbf{M}_{pq})^2}{2}}. \tag{4}$$

The MT decomposition used here is $\mathbf{M} = \mathbf{M}_{\mathrm{ISO}} + \mathbf{M}_{\mathrm{DEV}}$, in which $\mathbf{M}_{\mathrm{ISO}}$ and $\mathbf{M}_{\mathrm{DEV}}$ stand for the ISO and deviatoric part, respectively, and $\mathbf{M}_{\mathrm{DEV}} = \mathbf{M}_{\mathrm{DC}} + \mathbf{M}_{\mathrm{CLVD}}$ (e.g., Julian *et al.*, 1998, p. 530). The relative size of the ISO, DC, and CLVD components is expressed in percentages, and the sum of their absolute values is 100%. The so-called deviator formulation assumes $\mathbf{M} = \mathbf{M}_{\mathrm{DEV}}$, and in this case the sum of DC and CLVD percentages is 100%. The definition of the percentages has not yet been unified in the literature; we follow equations (8a)–(8c) of Vavryčuk (2001).

The source of finite extent and duration is approximated by a point source (centroid). Assuming that the centroid position and centroid time are known, the displacement at a station can be written as

$$u_i(t) = \sum_{j}^{6} a_j \left(\sum_p \sum_q \mathbf{M}^j_{pq} * \mathbf{G}_{ip,q} \right) = \sum_{j=1}^{6} a_j \mathbf{E}^j_i(t) \tag{5}$$

(Aki and Richards, 2002). Here, $\mathbf{G}$ is Green's tensor and $\mathbf{E}^j$ denotes the jth elementary seismogram corresponding to the jth elementary MT. The Green's functions are calculated in 1D velocity models by the discrete wavenumber method (Bouchon, 1981), including near-field terms. Full displacement waveforms are inverted without any phase separation. Artificial time shifts of complete seismograms, sometimes used to compensate for deficiencies of the velocity model, are not used because we consider their application poorly justified (Zahradník *et al.*, 2008). We suppose that the moment-rate function is a delta function, which is a good approximation at frequencies below the corner frequency of the event. Then, equation (5) can be understood as a linear inverse problem for unknown a, hence, the unknown $\mathbf{M}$. The full-MT inversion seeks the value of all six a's, whereas the deviatoric inversion (DEV) assumes $a_6 = 0$; therefore, only the first five a's are calculated. The inverse problem is solved by the least-squares method. If the centroid position and time belong to the unknown parameters, they are sought through a spatiotemporal grid search in vicinity of a previously estimated position, and (together with $\mathbf{M}$) they collectively represent the CMT solution. The grid search maximizes the correlation between the observed (u) and synthetic (s) seismograms, defined by

$$\mathrm{Corr} = \frac{\int us}{\sqrt{\int u^2 s^2}}, \tag{6}$$

in which $\int us = \sum_i \int u_i(t) s_i(t) dt$ and summation is over components and stations. The match between the observed and synthetic seismograms is measured by the global variance reduction (VR):

$$\mathrm{VR} = 1 - \frac{\int (u-s)^2}{\int u^2} = \mathrm{Corr}^2. \tag{7}$$

This equation follows from equation (6) and from the fact that if synthetics s are found by the least-squares misfit minimization of $\int (u-s)^2$, then $\int us = \int ss$ (see, e.g., equations 1–6 of Kikuchi and Kanamori, 1991).

To examine how well or ill posed the inverse problem is, we additionally use the condition number (CN, equation 18 of Křížová *et al.*, 2013). It is a relative measure; a larger CN signalizes a worse (less stable) resolvability of MT. To measure the angular departure of any two DC solutions, under comparison, we use the Kagan angle (Kagan, 1991). The solutions are comparable (quite similar) if the angle is $<10°$–$20°$ (e.g., see Zahradník and Custódio, 2012). We implemented this method using ISOLA software (Sokos and Zahradník, 2008, 2013).

Technical Details

Before instrumental correction and band-pass filtering, the integrated raw displacement data are always carefully checked to detect possible disturbances in an attempt to prevent harming the CMT inversion (Zahradník and Plešinger, 2005, 2010; Vackář *et al.*, 2015). The frequency range of the waveform inversion (e.g., 0.05–0.08 Hz) used in this article is quite standard for near-regional applications of a similar type, in which the low- and high-frequency limits are determined by the noise (either instrumental or natural) and by the ability to model observed data with existing velocity models, respectively. Following our previous work (Křížová *et al.*, 2013; their fig. 1b,c and table 2), we use two velocity models: the model proposed by Novotný *et al.* (2001; obtained from regional surface-wave dispersion) and the model of Dimitriadis *et al.* (2010; obtained from nonlinear inversion of travel times and applicable to the broader region of Santorini Island). Hereafter, they are called N-model and D-model, for brevity.

Data

Although we basically focus on synthetics tests, we start with real data because in the synthetics tests we will use the same source–station configuration. We investigate two shallow events of the south-central Aegean region: the 27 January 2012 M_w 5.3 Cretan Sea earthquake and the 26 June 2009 M_w 4.9 Santorini earthquake (Fig. 1a and 1b, respectively). For their preliminary agency reports, we refer to the European-Mediterranean Seismological Centre (EMSC) webpages (see Data and Resources). MT solutions for both of the events are also available online (see Data and Resources). The Cretan Sea earthquake is the strongest event of the January 2012 earthquake sequence in Cretan Sea. The Santorini earthquake is the strongest event of the June 2009 earthquake sequence near Santorini Island.

The selection of the two events is motivated by the following:

1. both events were well recorded by broadband instruments of a reasonable azimuthal coverage;
2. both events occurred at a region where tectonic and volcanic events occur, making them candidates for possibly large ISO components;
3. these two earthquakes were previously studied by Kiratzi (2013) and Křížová *et al.* (2013), and so a good preliminary estimate of their parameters is available;
4. the previous analyses have revealed that the events may have a quite different ISO content, in particular a large ISO during the Santorini earthquake.

Table 1 summarizes standard CMT parameters of the events, calculated here, inverting only for the deviatoric part of the tensor, using the N-model, and the station configuration of Figure 1. In the following, first we make synthetic tests and demonstrate how the MT calculation is affected by neglecting the ISO component. Then, we try to find and show similar effects on real data. For both cases, we assume a fixed horizontal position of the centroid, varying only the depth.

Results: Synthetic Data

Motivation of the synthetic tests comes from observatory practice. Besides the centroid position and the strike/dip/rake angles, we are often interested in the DC% because this is the simplest parameter characterizing a possible deviation of the earthquake from pure shear faulting. We seek to understand how the obtained DC% depends on the adopted MT-inversion mode.

Moment Tensor

Consider a target earthquake of a full-MT $\mathbf{M} = \mathbf{M}_{\mathrm{ISO}} + \mathbf{M}_{\mathrm{CLVD}} + \mathbf{M}_{\mathrm{DC}}$. If we invert waveforms corresponding to this $\mathbf{M}$ under the assumption that the MT is purely deviatoric, we obtain $\mathbf{M}' = \mathbf{M}'_{\mathrm{CLVD}} + \mathbf{M}'_{\mathrm{DC}}$. It is obvious that, in general, $\mathbf{M}'_{\mathrm{CLVD}}$ does not equal $\mathbf{M}_{\mathrm{ISO}} + \mathbf{M}_{\mathrm{CLVD}}$; therefore, $\mathbf{M}'_{\mathrm{DC}}$ does not equal $\mathbf{M}_{\mathrm{DC}}$. Thus, we get a biased estimate of the DC%. How large is the DC% bias, and how does it depend on the size of the ISO component (ISO%)? These are the questions we are interested in. A related question is how the other source parameters, such as the strike/dip/rake angles and the centroid depth, may differ between the full-MT and deviatoric-MT inversion modes.

Designing the Synthetic Tests

All tests have a common feature. We calculate synthetic waveforms for an assumed centroid position and for a given

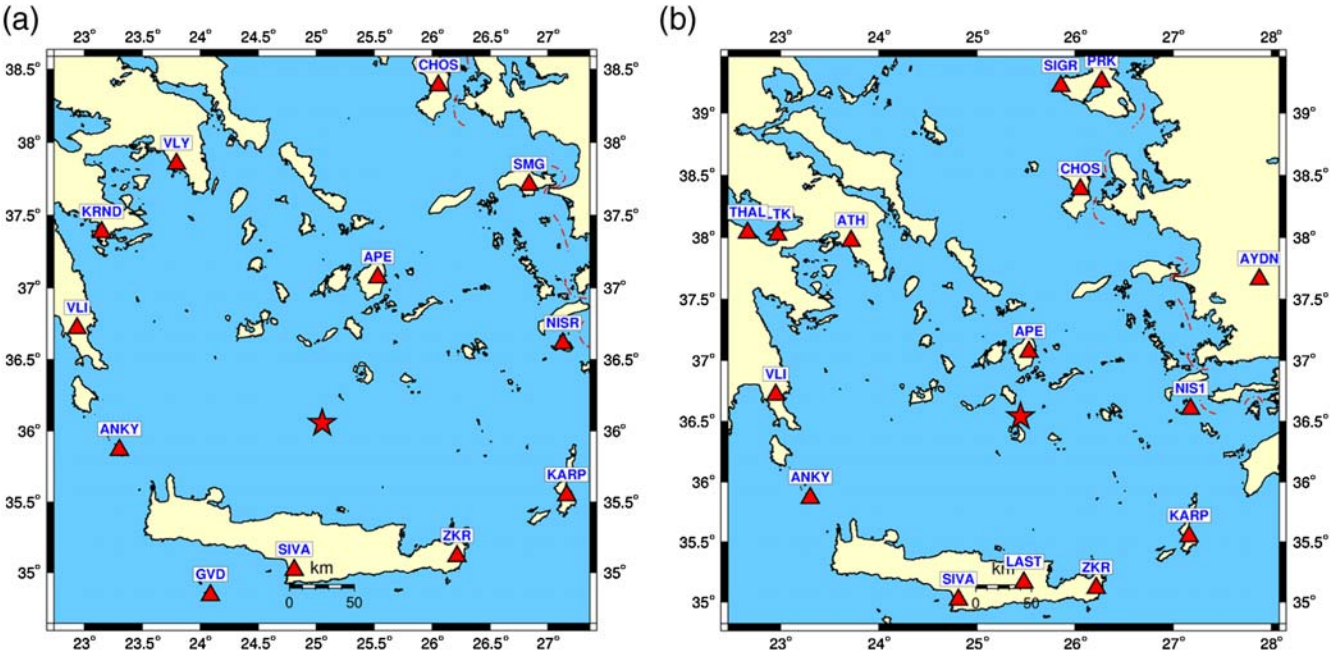

Figure 1. Studied earthquakes (asterisks) and stations (triangles) used in our analysis for (a) Cretan Sea and (b) Santorini. Table 1 provides more information on the earthquakes. The color version of this figure is available only in the electronic edition.

full MT. We then invert the synthetic waveforms in either a full-MT or deviatoric-MT mode and we leave the centroid depth and time free. We investigate the effects of the deviatoric constraint on the obtained source parameters (strike/dip/rake, depth, DC%, etc.). Three tests are made (A–C), each one with six subtests (1–6).

Tests A and B (Tables A3 and A4) differ in the centroid depth and strike/dip/rake angles of the simulated events, corresponding to the two selected real earthquakes. The subtests differ in their ISO% (rounded to integer values): ±90, ±46, and ±30 for test A and ±90, ±48, and ±32 for test B. The plus and minus signs correspond to explosion and implosion, respectively. For simplicity, all models have CLVD% = 0. Synthetic data are forward simulated and inverted using the same velocity model (N-model), unless differently specified.

Table 1

Earthquake Centroid Moment Tensor (MT) Parameters of the Cretan Sea Earthquake and Santorini Earthquake Calculated in This Work

	Earthquakes	
	Cretan Sea	Santorini
Date (yyyy/mm/dd)	2012/01/27	2009/06/26
Time (hh:mm:ss.s in UTC)	01:33:24.5	20:37:37.7
Latitude (°N)	36.056	36.540
Longitude (°E)	25.053	25.445
Depth (km)	8	4
M_w	5.3	4.6
M_0 (N·m)	1.18×10^{17}	1.07×10^{16}
Strike/dip/rake (°)	188/80/−112	243/59/−74
Strike/dip/rake (°)	76/24/−23	34/33/−114
DC*	94.4	59.2
VR†	64.2	64.5

*DC, percentage of double couple.
†VR, variance reduction in percent.

Technically, the subtests are created as follows: we choose the strike/dip/rake angles and calculate the a-coefficients $a_1, \ldots, a_5$ of the deviatoric MT (see equation 3). Then, we create full MTs of several ISO components by choosing appropriate values of the sixth coefficient a_6 (Tables A1 and A2). For synthetics tests, we have chosen $a_1, \ldots, a_5$ coefficients that are close to solutions for full-MT inversions in real cases (it is because we are changing the ISO component across subtests; therefore, full-MT inversion was used). The true depth for test A is 8 km (Table 2) and for test B is 6 km (Table 3). The 6 km depth is preferred because the former 4 km depth (Table 1) was calculated for deviatoric solution only.

Test C is more complicated (Table A5). The assumed source parameters are as in test B (Tables A1 and A2); however, to illustrate possible effects of inaccurate velocity models, we forward simulate synthetic waveforms in one model (N-model), but invert them in the other (D-model). That is why in test C, variance reduction (equation 7) is always less than 85%.

The MT-inversion results for synthetic tests A–C (Figs. 2–6) including the subtests 1–6, mentioned in corresponding Tables A3–A5, reveal a number of interesting features, which are discussed in the following sections.

Focal Mechanism

First, we focus on the fault-plane solution by looking at the nodal lines. These lines are the result of the inversion

Table 2
Cretan Sea Earthquake

Earthquake	DC	CLVD	ISO	CN	VR (%)	Depth (km)	Strike (°)	Dip (°)	Rake (°)
N (full)	83.2	7.2	−9.6	2.56	64.5	8	187	81	−113
							79	24	−20
N (deviatoric)	94.4	5.6	0.0	2.03	64.2	8	188	80	−112
							76	24	−23

Inversion is in full-MT and deviatoric-MT modes. N, N-model; ISO, isotropic; CN, condition number; CLVD, compensated linear vector dipole.

(subtests 1–6, mentioned in corresponding Tables A3–A5). For full-MT inversion in test A, we see (Fig. 2a) that these nodal lines do not significantly change for all subtests 1–6. A similar result is obtained for test B (Fig. 2c). In most subtests of test A (Fig. 2b), the nodal lines of the deviatoric inversion differ only marginally from the correct solution. However, there are two exceptions, corresponding to the MT with the largest ISO ± 89.5%. For these cases, the deviatoric inversion produces an MT whose CLVD is greater than 90%, and the fault-plane solution of the deviatoric inversion differs quite significantly from the correct one. The deviation, expressed in terms of the Kagan angle, is 47° and 37° for ISO = −89.5% and +89.5%, respectively. On the other hand, for ISO = ±29.8%, the Kagan angle is smaller than 10°. The subtests of test B (Fig. 2d), representing a similar experiment but with different strike/dip/rake angles and a slightly shallower depth, give almost the same results (see Tables A3–A5 for details).

In test C, where the inversion is performed for the incorrect velocity model, we obtain deviations from the correct solution even in the full-MT inversion (Fig. 2e). The latter is the case of subtests C1D and C2D, with real ISO = −90.3% and +90.4% in which we obtain only ISO = −70.1 and +75.1, respectively. For subtest C2D (full), we get a Kagan angle as large as 91°. For two smaller (absolute) values of ISO, the full-MT inversion gives a higher variance reduction and small Kagan angle. The deviatoric inversion in the incorrect model (Fig. 2f) provides relatively small deviation of the nodal lines from the correct solution. It means that, in this example, the inversion of the fault-plane solution is robust.

DC% and Depth

We seek to see how much the DC% deviates from the correct values when neglecting the ISO source component during the MT inversion. This question is answered in Figure 3a. The prescribed (correct) values are shown by filled circles for test A and filled squares for tests B and C, which differ across subtests 1–6. We should mention that we generate synthetic data without noise and then invert them, which is why the results for full-MT inversion in the N-model are considered to be correct. The performance of test A is easy to understand. In most subtests 1–6 with variable ISO% of the input data, the DC% is well reproduced in the deviatoric inversion (empty circles near the filled circles) because ISO% is projected into CLVD%, thus keeping the correct DC%, except in two cases. The two exceptions, subtests 3 and 5, correspond to the input ISO of −46% and −30%, which did not project into CLVD, but instead they apparently enriched the DC source content, that is increased DC%. The enrichment is so high that the resulting DC% of subtests 3 and 5 is practically the same (> 90%), not reflecting the different DC% of the input data. We also note that in all the subtests, the retrieved DC% never drops below the true value. Values of the Kagan angle are shown in Figure 3b, and the source depth was changed due to the deviatoric assumption (Fig. 3c). The results of test B are analogous to test A (marked in Fig. 3a with filled and empty squares, respectively).

Test C (also in Fig. 3a,b), in which the inversion is done intentionally with a different velocity model than the one used to produce the synthetic data, is more complicated. Both velocity models are described in figure 1b,c and table 2 of Křížová *et al.* (2013). The prescribed (correct) values are those of test B due to the incorrect velocity model, in this case test C. For the deviatoric-MT inversion, the DC% is almost always biased for the low input DC% (subtest 1, also accompanied by an erroneous retrieved depth). However, for the full-MT inversion the retrieved DC% is relatively close to the true one (or somewhat lower). The DC% for the full-MT inversion is retrieved well in subtests 1 and 2, but in subtests 3–6 it is lower than the true value. Our results show that an incorrect velocity model introduces bias in estimating the DC% in both the full-MT and deviatoric-MT inversions.

Correlation versus Source Depth

Here, we analyze whether there is any simple feature in these complex results, at least for some specific values of ISO%. As seen in Figures 2 and 3, subtests 1 and 2 of the largest ISO% seem to behave differently in all aspects (the fault-plane solution, DC%, depth). Therefore, we further concentrate on the variation of the waveform correlation with trial source depth, and we will show that indeed the events with a large ISO% may have a specific correlation-depth behavior. Recall that the source depth prescribed in synthetic data is 8 km for test A and 6 km for tests B and C. Synthetic seismograms created for the full-MT source at these depths are inverted either in the full-MT or deviatoric-MT mode, while the trial depth is free (tests A–C in Figs. 4–6).

Synthetic Data Inverted in Full-MT Mode

We start with the synthetic data inverted in full-MT mode, and, as seen from the correlation-depth curves (Figs. 4a, 5a, and 6a), no pronounced local maxima can be detected. In other words, for this particular event–station geometry and velocity

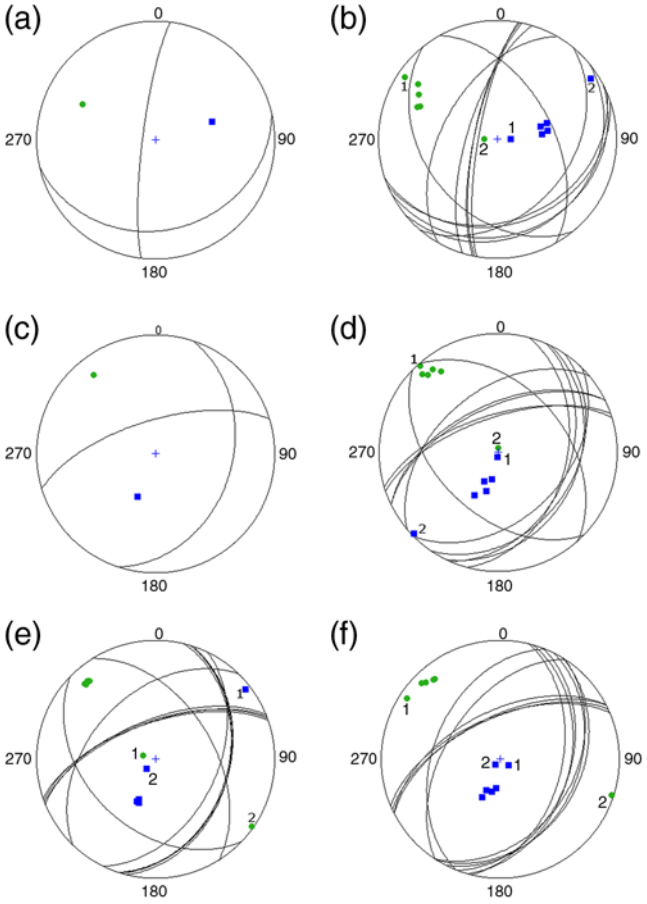

Figure 2. Nodal lines are the result of the inversion (subtests 1–6). Squares are symbols for P-axis and circles stands for T-axis. (a) Test A, full moment tensor (MT); (b) test A, deviatoric MT; (c) test B, full MT; (d) test B, deviatoric MT; (e) test C, full MT; (f) test C, deviatoric MT. (Each inversion is made in full-MT mode [a,c,e] and deviatoric-MT mode [b,d,f]. For b, d, e, and f, we marked P-axis and T-axis for subtests 1 and 2.) The color version of this figure is available only in the electronic edition.

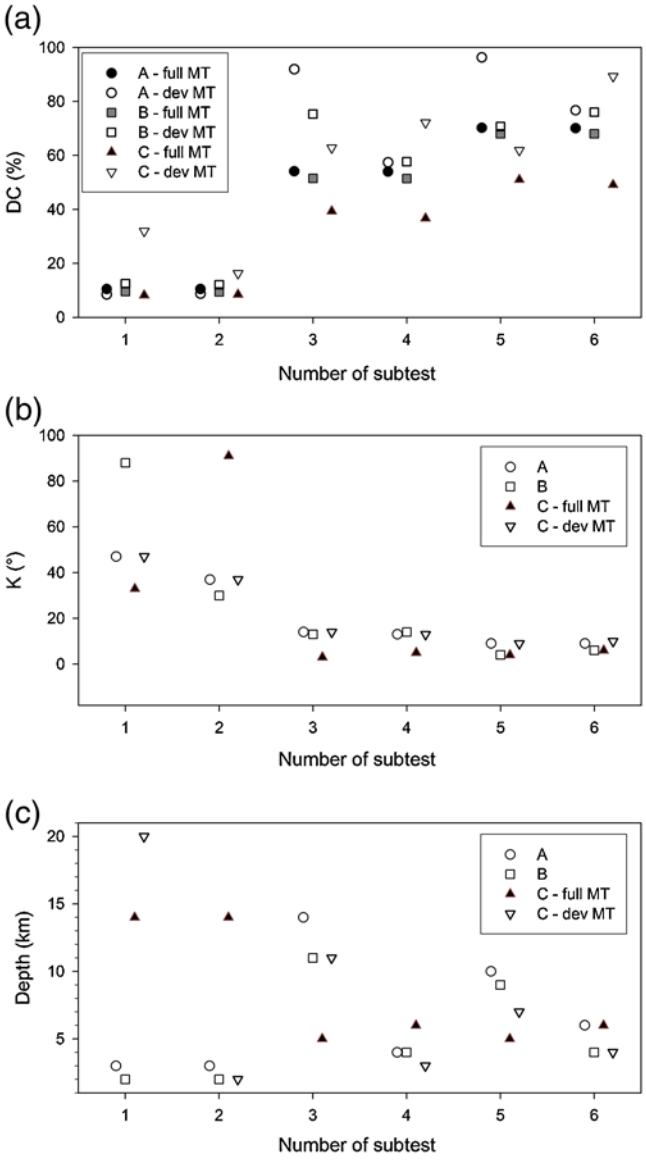

Figure 3. Results corresponding to Tables A3–A5. (a) Double-couple percentage (DC%): the input data (the correct solution) are mentioned, such as full MT in N-model. The remaining symbols, explained in legend, are the result of the inversion (subtests 1–6). (b) Kagan angle: for tests A and B is the difference between full MT and deviatoric (dev) MT and for test C is the difference between full MT for B and results from inversion in wrong velocity model. (c) Source depth obtained for each subtest. The color version of this figure is available only in the electronic edition.

model, the centroid depth resolvability is almost none. The (weak) depth variation is almost independent of ISO%. There is a weak dependence on depth for subtests 3–6, but the shape of curves is almost the same. The correlation seems to be least dependent on depth in subtests 1 and 2; the curves (with circles) are almost flat. Note an interesting feature of Figure 6a (the same MT as in Fig. 5a, but the full-MT inversion is made with the wrong velocity model): despite the use of the inappropriate velocity model, the depth dependence in Figure 6a has a similar shape as in Figure 5a, only the correlation values are lower.

Synthetic Data Inverted in Deviatoric-MT Mode

The inversion of the same synthetic data in deviatoric-MT mode (Figs. 4b, 5b, and 6b) clearly shows that neglecting the ISO component has a strong effect upon the correlation-depth variations. In particular, subtests 1 and 2 show very deep local minima, but weaker local minima can also be observed in the other subtests. The minima are close (but not identical) to the true source depth. This remarkable feature is common to tests A–C. The tests indicate that if a real event has a very large ISO% (low DC%), the correlation-depth graph may get an apparent minimum near the correct source depth, that is, the depth will be incorrectly determined. For example, as in Figures 4b and 5b, the source depth can be erroneously identified with the local correlation maximum at a depth < 5 km.

The significantly different correlation-depth profiles can be simply explained. Imagine a source at depth D with a large ISO component and negligible CLVD. This ISO component constitutes a significant part of the waveforms. In the

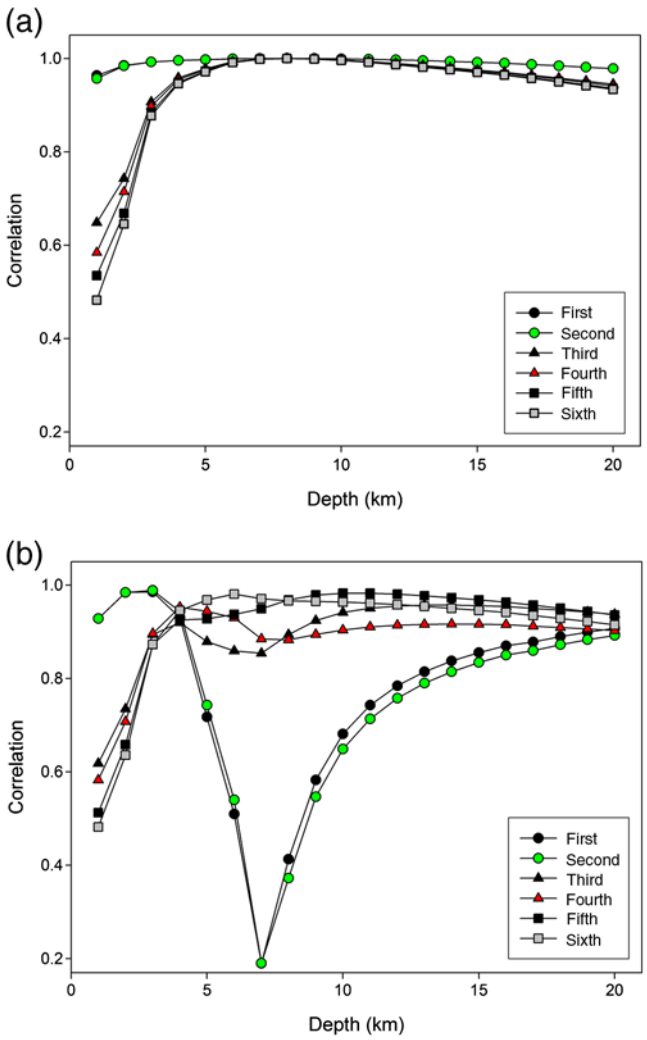

Figure 4. Waveform correlation for synthetic test A (subtests are for variable isotropic percentage [ISO%], see legend and Table A3). Correct source depth is 8 km. Synthetic waveforms due to full MT are inverted in two modes: (a) full MT and (b) deviatoric MT. The color version of this figure is available only in the electronic edition.

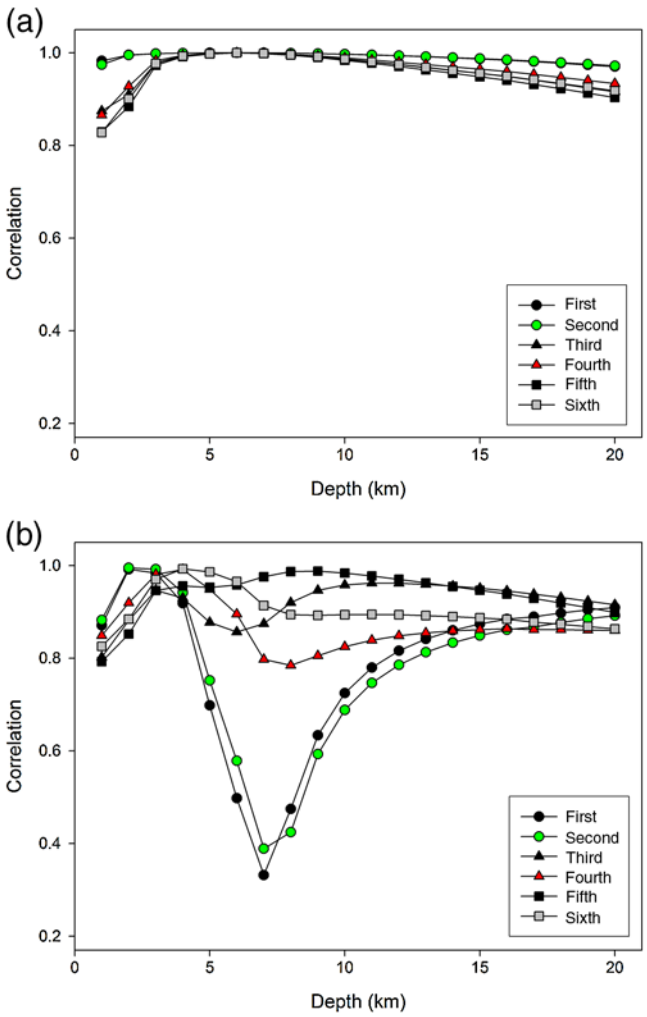

Figure 5. Waveform correlation for synthetic test B (subtests are for variable ISO%, see legend and Table A4). Correct source depth is 6 km. Synthetic waveforms due to full MT are inverted in two modes: (a) full MT and (b) deviatoric MT. The color version of this figure is available only in the electronic edition.

full-MT inversion, the waveforms can be best fitted at depth D. However, in the deviatoric-MT inversion, the true waveforms are approximated with synthetics lacking the ISO part. It means that real data are interpreted in terms of an inappropriate model (DC and CLVD only), thus deteriorating the match at depth D. Because the inappropriate model does not contain ISO, real data could be partially fit only by a source model at depth D having a different focal mechanism, biased with respect to the true one in a way compensating the missing ISO. However, if no biased deviatoric MT can compensate the lack of ISO, a correlation minimum is created. At another trial depth, $D' \neq D$, some deviatoric-MT source model can exist (e.g., a model with a spurious CLVD, and/or with biased strike, dip, and rake angles) that produces synthetics fitting real data almost as well as the full-MT synthetics at depth D. Hence, the source depth estimate in the deviatoric-MT inversion may be biased from D to D'.

The previously detailed synthetic tests have some practical implications. We think that the message of the synthetic tests is quite strong. They suggest that if the data processing indicates a small DC%, the correlation-depth analysis should be made twice, both in the full-MT and deviatoric-MT modes. If these two results strongly differ from each other, they may indicate the presence of a large ISO component. More sophisticated methods (e.g., Křížová *et al.*, 2013) may then be applied as a next step toward checking relevance of the large ISO%.

Results: Real Data

The inversion results using the observed waveforms from the two earthquakes as introduced in Table 1 are summarized in Tables 2 and 3 and Figures 7 and 8 for the Cretan Sea and Santorini Island events, respectively. To more deeply investigate possible non-DC components, we follow the approach of the Synthetic Data Inverted in Deviatoric-MT

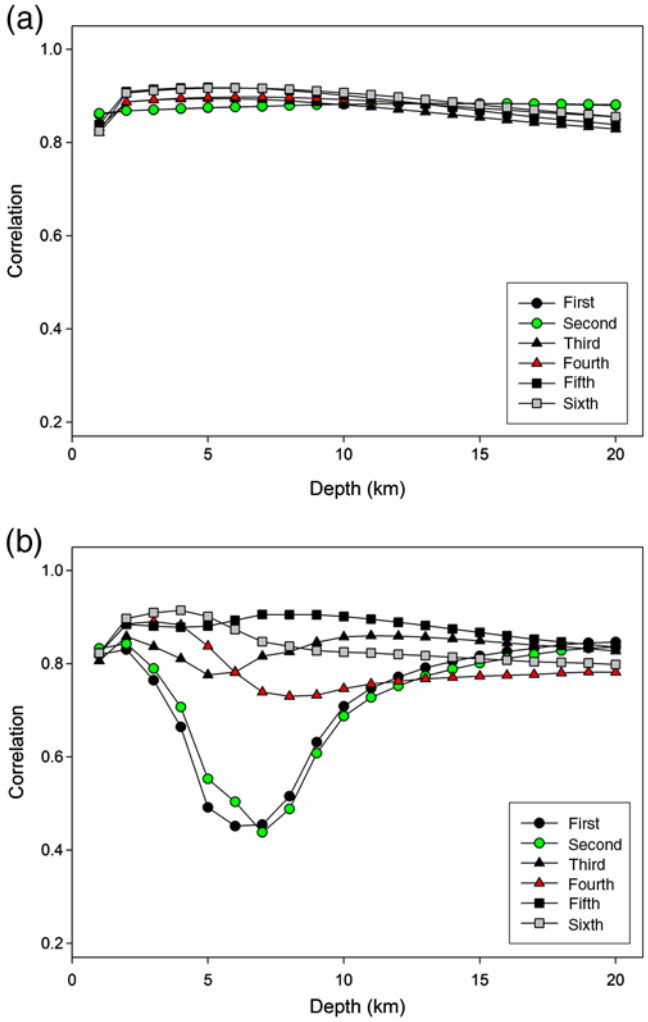

Figure 6. As in Figure 5, but the inversion is made in a different model (D-model, whereas the forward simulation used N-model; see legend and Table A5). (a) Full MT. (b) Deviatoric MT. The color version of this figure is available only in the electronic edition.

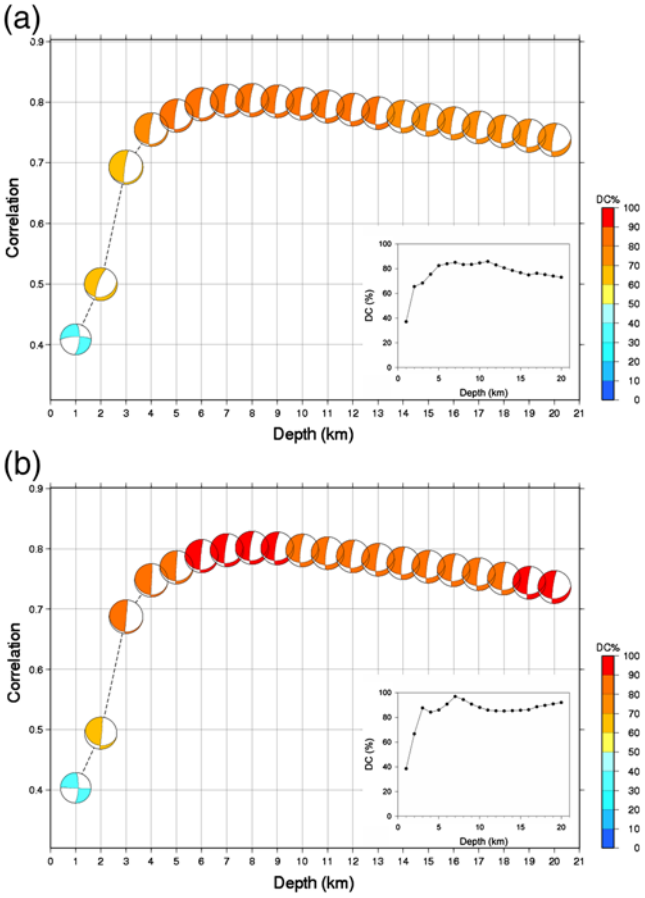

Figure 7. Waveform correlation for the Cretan Sea earthquake. Real waveforms are inverted in two modes: (a) full MT and (b) deviatoric MT. The color version of this figure is available only in the electronic edition.

Mode section and study the depth-dependent correlation in two modes: full and deviatoric. For the Cretan Sea earthquake, our CLVD value (6%) is smaller than the CLVD value (43%) obtained in previous modeling, using a different code and station geometry (Kiratzi, 2013). For the Santorini earthquake, we expect a large ISO component because standard deviatoric CMT inversion indicated a DC% as low as 59%. Two velocity models for Santorini earthquake were used (D-model and N-model), but the results are similar; thus we present in Figure 8 only the latter.

The two events are very different. The Cretan Sea has a large DC% for both inversion modes in a broad range of the trial source depths, and the correlation-depth variations are almost identical. These are indications of a low ISO component. The Santorini earthquake has a lower DC% at the depths where the correlation takes its maximum values. Most importantly, the full-MT and deviatoric-MT inversions provide considerably different correlation-depth dependences. For the Santorini earthquake, we obtain a weak correlation maximum at a depth of 6 km in the full-MT mode, contrasting with a very pronounced local minimum in the deviatoric-MT mode at a depth of 8 km, and also featuring a local maximum at a depth of 4 km. Compared with the synthetic tests, we interpret these features as an indicator for a large ISO component of the Santorini Island event. On the other hand, the missing local minimum in correlation function for the Cretan Sea earthquake indicates a relatively low ISO component. We also believe that the correlation maximum at 4 km is a biased estimate of the centroid depth; the true depth could be closer to 6–8 km. The present conclusion of the large ISO% of the Santorini earthquake is in good agreement with the independently obtained results of Křížová *et al.* (2013).

Conclusions

For any earthquake, we may apply several methods attempting to resolve its CMT and to estimate its uncertainty. Although the CMT calculations belong to routine tasks, the uncertainty estimate is more of a research problem, particularly regarding the ISO component. This work provides a hypothesis that some simple tools, applicable in the routine MT inversion,

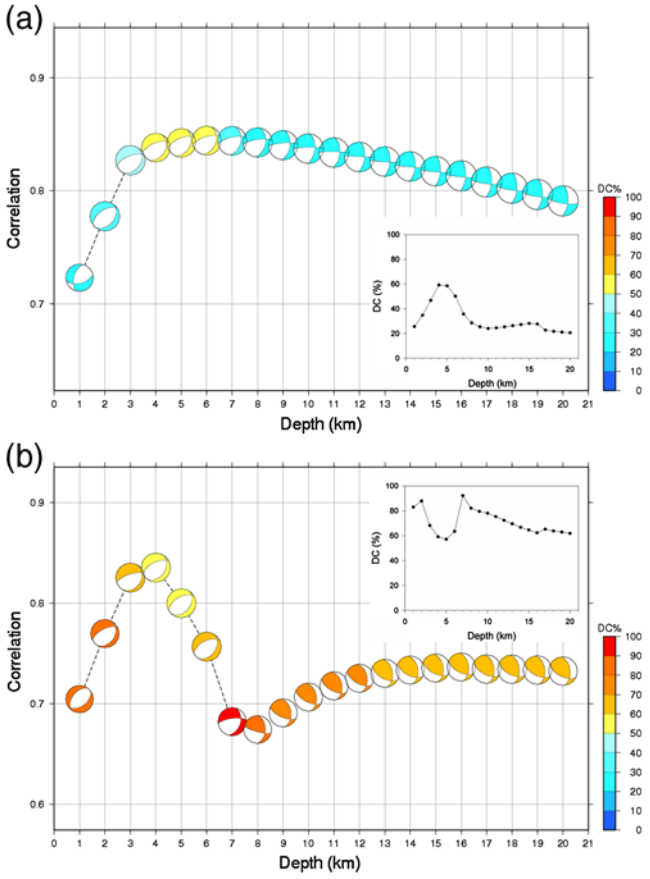

Figure 8. Waveform correlation for the Santorini earthquake. Real waveforms are inverted in two modes: (a) full MT and (b) deviatoric MT. The color version of this figure is available only in the electronic edition.

could relatively easily identify earthquakes with strong ISO, which can be used in routine seismological practice.

Our recommendation is as follows: if routine processing of an earthquake indicates a small DC%, then the waveform inversion should be made in two modes: the full MT and the deviatoric MT. The processing should include a careful examination of the waveform correlation as a function of the trial centroid depth. If the two inversion modes (full and deviatoric) provide remarkably different correlation-depth functions, and in particular, if the correlation of the deviatoric inversion poses a deep local minimum, although in the full-MT inversion such a minimum is absent, we have an indication of a strong ISO component. The likely source depth is close to that local minimum. Because in routine practice just the maximum of the correlation-depth function provides an estimate of the centroid depth, here we see that in case of the deviatoric inversion of an event with large ISO this traditional approach fails. In this sense, deviatoric inversions of events with large ISO components should be applied with caution because the maximum of the correlation-depth function may return an incorrect depth (and possibly also an incorrect fault-plane solution).

This hypothesis has been supported by extensive synthetic tests. Interestingly, the tests indicated that the mentioned features of the correlation-depth functions of the events with large ISO components (i.e., deep local minima present in the deviatoric-MT inversion but absent in the full-MT inversion) are rather robust. Indeed, these characteristic features were found even in the case when synthetic waveforms simulated in one velocity model were inverted in another model available for the same region.

Our approach has been tested on two shallow earthquakes in Greece, the 27 January 2012 M_w 5.3 Cretan Sea event and the 26 June 2009 M_w 4.9 Santorini event. Their behavior was quite different, indicating a significantly stronger ISO component for the Santorini earthquake. This indication is in agreement with the previously detailed analysis of the large ISO, made with a more complex research tool (Křížová *et al.*, 2013).

As a final remark, we propose that the events indicated in the standard CMT processing as potential candidates for large ISO (using our proposed approach) be further analyzed by more sophisticated methods.

Data and Resources

Broadband waveforms were retrieved from the permanent stations of the Hellenic Unified Seismic Network (HUSN), operated jointly by the National Observatory of Athens (NOA, doi: 10.7914/SN/HL), the Aristotle University of Thessaloniki (AUTH, doi: 10.7914/SN/HT), the University of Patras (UPSL, doi: 10.7914/SN/HP), and the University of Athens (UOA). The records from one station of the National Seismic Network of Turkey (DDA) were also used. A number of UPSL stations are co-operated by

Table 3
Santorini Earthquake

Earthquake	DC	CLVD	ISO	CN	VR	Depth (km)	Strike (°)	Dip (°)	Rake (°)
N (full)	50.2	1.4	48.4	3.90	65.7	6	253	67	−61
							18	35	−139
N (deviatoric)	59.2	40.8	0.0	3.20	64.5	4	243	59	−74
							34	33	−114
D (full)	52.5	4.4	43.1	3.64	69.4	5	250	65	−65
							21	34	−132
D (deviatoric)	60.4	39.6	0.0	3.38	69.0	3	246	62	−73
							33	31	−119

Inversion is in full-MT and deviatoric-MT modes. N, N-model; D, D-model.

the Charles University in Prague. Software ISOLA (Sokos and Zahradník, 2008) was used to calculate the moment tensors. The Green's functions in ISOLA were computed using the AXITRA code of Coutant (1989). The Generic Mapping Tools (GMT; Paul Wessel and Walter H. F. Smith, http://gmt.soest.hawaii.edu/, last accessed July 2016) and MATLAB (http://www.mathworks.com/products/matlab/, last accessed July 2016) were also used. Preliminary agency reports, including moment tensor solutions, are mentioned on the European-Mediterranean Seismological Centre (EMSC) webpages (www.emsc-csem.org/, last accessed July 2016).

Acknowledgments

Partial financial support of this work was obtained from the Czech Science Foundation Grant Number GACR-14-04372S. We also acknowledge partial support from THALES project (MIS377335), funded by the European Union (European Social Fund, ESF) and Greek national funds. The comments and suggestions of C. P. Evangelidis are gratefully acknowledged.

References

Aki, K., and P. G. Richards (2002). *Quantitative Seismology*, University Science Books, Sausalito, California, 704 pp.

Bouchon, M. (1981). A simple method to calculate Green's functions for elastic layered media, *Bull. Seismol. Soc. Am.* **71,** 959–971.

Cesca, S., A. Rohr, and T. Dahm (2013). Discrimination of induced seismicity by full moment tensor inversion and decomposition, *J. Seismol.* **17,** no. 1, 147–163.

Coutant, O. (1989). Program of numerical simulation AXITRA, *Res. Rept.* LGIT, Grenoble, France (in French).

Dimitriadis, I., C. Papazachos, D. Panagiotopoulos, P. Hatzidimitriou, M. Bohnhoff, M. Rische, and T. Meier (2010). *P* and *S* velocity structures of the Santorini–Coloumbo volcanic system (Aegean Sea, Greece) obtained by non-linear inversion of travel times and its tectonic implications, *J. Volcanol. Geoth. Res.* **195,** 13–30.

Dufumier, H., and L. Rivera (1997). On the resolution of the isotropic component in moment tensor inversion, *Geophys. J. Int.* **131,** 595–606.

Ford, S. R., D. S. Dreger, and W. R. Walter (2009). Identifying isotropic events using a regional moment tensor inversion, *J. Geophys. Res.* **114,** no. B1, doi: 10.1029/2008JB005743.

Foulger, G. R., B. R. Julian, D. P. Hill, A. M. Pitt, P. E. Malin, and E. Shalev (2004). Non-double-couple microearthquakes at Long Valley Caldera, California, provide evidence for hydraulic fracturing, *J. Volcanol. Geoth. Res.* **132,** no. 1, 45–71.

Horálek, J., J. Šílený, and T. Fischer (2002). Moment tensors of the January 1997 earthquake swarm in NW Bohemia (Czech Republic): Double-couple vs. non-double-couple events, *Tectonophysics* **356,** no. 1, 65–85.

Julian, B. R., A. D. Miller, and G. R. Foulger (1998). Non-double-couple earthquakes: 1. Theory, *Rev. Geophys.* **36,** 525–549.

Kagan, Y. Y. (1991). 3-D rotation of double-couple earthquake sources, *Geophys. J. Int.* **106,** 709–716, doi: 10.1111/j.1365-246X.1991.tb06343.x.

Kawakatsu, H. (1996). Observability of the isotropic component of a moment tensor, *Geophys. J. Int.* **126,** no. 2, 525–544.

Kikuchi, M., and H. Kanamori (1991). Inversion of complex body waves. III, *Bull. Seismol. Soc. Am.* **81,** 2335–2350.

Kiratzi, A. (2013). The January 2012 earthquake sequence in the Cretan Basin, south of the Hellenic Volcanic Arc: Focal mechanisms, rupture directivity and slip models, *Tectonophysics* **586,** 160–172, doi: 10.1016/j.tecto.2012.11.019.

Křížová, D., J. Zahradník, and A. Kiratzi (2013). Resolvability of isotropic component in regional seismic moment tensor inversion, *Bull. Seismol. Soc. Am.* **103,** no. 4, 2460–2473, doi: 10.1785/0120120097.

Minson, S. E., and D. S. Dreger (2008). Stable inversions for complete moment tensors, *Geophys. J. Int.* **174,** no. 2, 585–592.

Mustać, M., and H. Tkalčić (2016). Point source moment tensor inversion through a Bayesian hierarchical model, *Geophys. J. Int.* **204,** no. 1, 311–323, doi: 10.1093/gji/ggv458.

Novotný, O., J. Zahradník, and G.-A. Tselentis (2001). Northwestern Turkey earthquakes and the crustal structure inferred from surface waves observed in western Greece, *Bull. Seismol. Soc. Am.* **91,** 875–879.

Shuler, A., G. Ekström, and M. Nettles (2013). Physical mechanisms for vertical-CLVD earthquakes at active volcanoes, *J. Geophys. Res.* **118,** 1569–1586, doi: 10.1002/jgrb.50131.

Silver, P. G., and T. H. Jordan (1982). Optimal estimation of scalar seismic moment, *Geophys. J. R. Astron. Soc.* **70,** 755–787, doi: 10.1111/j.1365-246X.1982.tb05982.x.

Sokos, E., and J. Zahradník (2013). Evaluating centroid moment tensor uncertainty in new version of ISOLA software, *Seismol. Res. Lett.* **84,** 656–665.

Sokos, E. N., and J. Zahradník (2008). ISOLA a Fortran code and a MATLAB GUI to perform multiple-point source inversion of seismic data, *Comput. Geosci.* **34,** 967–977.

Song, F., and M. N. Toksöz (2011). Full-waveform based complete moment tensor inversion and source parameter estimation from downhole microseismic data for hydrofracture monitoring, *Geophysics* **76,** no. 6, WC103–WC116.

Templeton, D. C., and D. S. Dreger (2006). Non-double-couple earthquakes in the Long Valley volcanic region, *Bull. Seismol. Soc. Am.* **96,** 69–79.

Tkalčić, H., D. S. Dreger, G. R. Foulger, and B. R. Julian (2009). The puzzle of the 1996 Bárdarbunga, Iceland, earthquake: No volumetric component in the source mechanism, *Bull. Seismol. Soc. Am.* **99,** 3077–3085.

Vackář, J., J. Burjánek, and J. Zahradník (2015). Automated detection of disturbances in seismic records; MouseTrap code, *Seismol. Res. Lett.* **86,** 442–450.

Vasco, D. W. (1990). Moment-tensor invariants: Searching for non-double-couple earthquakes, *Bull. Seismol. Soc. Am.* **80,** no. 2, 354–371.

Vavryčuk, V. (2001). Inversion for parameters of tensile earthquakes, *J. Geophys. Res.* **106,** 16,339–16,355.

Vavryčuk, V. (2004). Inversion for anisotropy from non-double-couple components of moment tensors, *J. Geophys. Res.* **109,** no. B07306, doi: 10.1029/2003JB002926.

Vavryčuk, V. (2011). Tensile earthquakes: Theory, modeling, and inversion, *J. Geophys. Res.* **116,** no. B12320, doi: 10.1029/2011JB008770.

Vavryčuk, V., M. Bohnhoff, Z. Jechumtálová, P. Kolář, and J. Šílený (2008). Non-double-couple mechanisms of microearthquakes induced during the 2000 injection experiment at the KTB site, Germany: A result of tensile faulting or anisotropy of a rock? *Tectonophysics* **456,** no. 1, 74–93.

Zahradník, J., and S. Custódio (2012). Moment tensor resolvability: Application to southwest Iberia, *Bull. Seismol. Soc. Am.* **102,** 1235–1254, doi: 10.1785/0120110216.

Zahradník, J., and A. Plešinger (2005). Long-period pulses in broadband records of near earthquakes, *Bull. Seismol. Soc. Am.* **95,** no. 5, 1928–1939.

Zahradník, J., and A. Plešinger (2010). Toward understanding subtle instrumentation effects associated with weak seismic events in the near field, *Bull. Seismol. Soc. Am.* **100,** 59–73.

Zahradník, J., J. Janský, and V. Plicka (2008). Detailed waveform inversion for moment tensors of M ~ 4 events: Examples from the Corinth Gulf, Greece, *Bull. Seismol. Soc. Am.* **98,** 2756–2771.

Appendix

Three synthetic tests were made (A–C), each one with six subtests (1–6). Tables A1 and A2 show the input data for

Table A1
a-Coefficients Used to Generate Moment Tensor (MT) Models

Parameter	Test A	Tests B and C
a_1	-0.494837×10^{17}	-0.379445×10^{16}
a_2	0.964645×10^{16}	0.450544×10^{16}
a_3	0.102082×10^{18}	0.613149×10^{14}
a_4	-0.934958×10^{16}	-0.228232×10^{16}
a_5	-0.201239×10^{17}	-0.195328×10^{16}

Table A2
a_6-Coefficients Used to Generate MT Models

Calculation	Test A	Tests B and C
1	-0.1×10^{19}	-0.1×10^{18}
2	0.1×10^{19}	0.1×10^{18}
3	-0.1×10^{18}	-0.1×10^{17}
4	0.1×10^{18}	0.1×10^{17}
5	-0.5×10^{17}	-0.5×10^{16}
6	0.5×10^{17}	0.5×10^{16}

these calculations. Tables A3–A5 are listed as a supplement to Figures 2–6.

Charles University
Faculty of Mathematics and Physics
V Holešovičkách 2
180 00 Prague 8, Czech Republic
dana.krizova@mff.cuni.cz
jiri.zahradnik@mff.cuni.cz
(D.K., J.Z.)

Aristotle University of Thessaloniki
Faculty of Sciences
Department of Geophysics
54124 Thessaloniki, Greece
kiratzi@geo.auth.gr
(A.K.)

Manuscript received 16 March 2016;
Published Online 18 October 2016

Table A3
Synthetic Test A. Data with Full MT Inverted in Full and Deviatoric Modes, Using Correct Velocity Model

Earthquake	DC	CLVD	ISO	CN	VR	Depth (km)	Strike (°)	Dip (°)	Rake (°)	K (°)*
A1N (full)	10.5	0.0	−89.5	2.56	99.98	8	186	81	−112	
							76	24	−21	
A1N (deviatoric)	8.5	91.5	0.0	3.81	97.00	3	331	52	96	47
							140	38	81	
A2N (full)	10.5	0.0	89.5	2.56	99.98	8	187	80	−112	
							76	24	−22	
A2N (deviatoric)	8.8	91.2	0.0	3.81	97.73	3	209	52	−96	37
							39	38	−82	
A3N (full)	54.1	0.0	−45.9	2.56	99.96	8	187	80	−112	
							76	24	−22	
A3N (deviatoric)	91.9	8.1	0.0	1.75	91.56	14	196	68	−113	
							67	33	−44	
A4N (full)	54.0	0.0	45.9	2.56	99.96	8	187	80	−112	14
							76	24	−22	
A4N (deviatoric)	57.4	42.6	0.0	2.57	90.69	4	191	74	−102	13
							51	20	−52	
A5N (full)	70.2	0.0	−29.8	2.56	99.95	8	187	80	−112	
							76	24	−22	
A5N (deviatoric)	96.3	3.7	0.0	1.54	96.52	10	191	74	−114	9
							70	28	−34	
A6N (full)	70.1	0.0	29.8	2.56	99.95	8	187	80	−112	
							76	24	−22	
A6N (deviatoric)	76.7	23.3	0.0	2.74	96.17	6	190	77	−106	9
							62	20	−39	

All calculations are for 12 stations. CLVD is stated in absolute value. DC, double couple; ISO, isotropic; CN, condition number; VR, variance reduction. Synthetic waveforms due to full MT are inverted under deviatoric constraint (ISO% = 0). The forward simulation and the inversion are made in same velocity model. Results for full MT for input data are put into the table for comparison. Subtests 1–6 differ in their ISO% values but share almost the same strike/dip, rake, and depth.

*K, Kagan angle (reference solution is the result for full MT in each subtest).

Table A4

Synthetic Test B. Data with Full MT Inverted in Full and Deviatoric Modes, Using Correct Velocity Model

Earthquake	DC	CLVD	ISO	CN	VR	Depth (km)	Strike (°)	Dip (°)	Rake (°)	*K* (°)*
B1N (full)	9.6	0.1	−90.3	3.90	99.95	6	252	66	−61	
							18	36	−138	
B1N (deviatoric)	12.5	87.5	0.0	4.42	98.23	2	318	42	93	88
							133	47	86	
B2N (full)	9.4	0.1	90.4	3.90	99.96	6	252	66	−60	
							18	36	−138	
B2N (deviatoric)	12.1	87.9	0.0	4.42	98.92	2	229	47	−86	30
							44	42	−93	
B3N (full)	51.5	0.1	−48.4	3.90	99.92	6	252	66	−61	
							18	36	−138	
B3N (deviatoric)	75.3	24.7	0.0	2.22	91.40	11	243	56	−65	13
							23	40	−122	
B4N (full)	51.4	0.1	48.5	3.90	99.94	6	252	66	−61	
							18	36	−138	
B4N (deviatoric)	57.7	42.3	0.0	3.20	97.87	4	244	58	−73	14
							34	34	−115	
B5N (full)	68.0	0.0	−31.9	3.90	99.91	6	252	66	−61	
							18	36	−138	
B5N (deviatoric)	70.7	29.3	0.0	2.31	96.96	9	252	64	−55	4
							14	42	−139	
B6N (full)	68.0	0.0	32.0	3.90	99.93	6	252	66	−61	
							18	36	−138	
B6N (deviatoric)	76.0	24.0	0.0	3.20	98.18	4	251	65	−67	6
							25	32	−130	

As in Table A3, but the input data (results for full-MT solution) have different strike/dip, rake, and depth than in test A. All calculations are for 15 stations (components with good signal-to-noise ratio are used).

*K, Kagan angle (reference solution is the result for full MT in each subtest)

Table A5

Synthetic Test C. Data with Full MT Inverted in Full and Deviatoric Modes Using Different Velocity Model

Earthquake	DC	CLVD	ISO	CN	VR	Depth (km)	Strike (°)	Dip (°)	Rake (°)	*K* (°)*
C1D (full)	8.2	21.7	−70.1	4.18	78.59	14	223	44	−76	33
							25	47	−102	
C1D (deviatoric)	32.0	68.0	0.0	2.82	71.17	20	202	42	−83	47
							13	47	−96	
C2D (full)	8.5	16.4	75.1	4.18	78.46	14	328	50	99	91
							133	40	78	
C2D (deviatoric)	16.3	83.7	0.0	5.17	71.17	2	213	51	−89	37
							32	38	−90	
C3D (full)	39.3	11.2	−49.5	3.64	79.32	5	251	65	−59	3
							17	38	−137	
C3D (deviatoric)	62.8	37.2	0.0	2.18	72.95	11	242	56	−64	14
							20	40	−123	
C4D (full)	36.7	13.8	49.5	3.02	79.72	6	248	65	−59	5
							14	38	−137	
C4D (deviatoric)	72.1	27.9	0.0	3.38	77.83	3	242	60	−73	13
							31	33	−116	
C5D (full)	51.0	15.5	−33.5	3.63	83.55	5	250	64	−60	4
							17	38	−135	
C5D (deviatoric)	61.9	38.1	0.0	2.59	81.56	7	247	61	−59	9
							16	41	−132	
C6D (full)	49.1	16.9	34.0	3.02	83.47	6	248	63	−60	6
							16	38	−134	
C6D (deviatoric)	89.3	10.7	0.0	3.10	82.50	4	245	61	−69	10
							26	34	−123	

Synthetic waveforms due to full MT are inverted under deviatoric constraint (ISO% = 0). The forward simulation was made in N-model and the inversion in D-model. Results for full-MT solution in N-model are in Table A4. Subtests 1–6 differ in their ISO% values but share the same strike/dip, rake, and depth, as also seen in test B. All calculations are for 15 stations (components with good signal-to-noise ratio are used).

*K, Kagan angle (reference solution is the result for full MT in N-model, mentioned in Table A4, in each subtest).